Transient bifurcation induced rocket acceleration leading to a relativistic bulk medium induced by designed high-intensity lasers

Ryutaro Matsui [1,2,*] and Yasuaki Kishimoto [1,2,3,†]

[1]*Graduate School of Energy Science, Kyoto University, Gokasho, Uji, Kyoto 611-0011, Japan*
[2]*Non-linear/Non-equilibrium Plasma Unit, Kyoto University, Gokasho, Uji, Kyoto 611-0011, Japan*
[3]*Institute of Advanced Energy, Kyoto University, Gokasho, Uji, Kyoto 611-0011, Japan*

(Received 22 August 2024; accepted 20 December 2024; published 31 January 2025)

By exploring a different function of plasma regulated by nonlinear waves and their transient bifurcations, we propose a boosting scheme for an object consisting of pure solid hydrogen medium irradiated by spatiotemporally designed high-intensity lasers to nearly the speed of light. This is achieved by two processes. One is the *slow process* via the formation of the shocklike structure in the medium and subsequent adiabatic compression exceeding 20 times the solid density to a width narrower than the local Debye length. This results in the *frozen-in dynamics* of the plasma regulated by the parameter ρ_e/γ_e ([electron charge density]/[electron relativistic factor]), which tends to be spatially less sensitive through the cancellation between laser ponderomotive and relativistic nonlinearities in a highly nonlinear regime. The other is the *fast process* of the transient bifurcation of the shock to a soliton leading to an *explosion*, which splits the structure into two shock structures propagating in opposite directions, i.e., one is boosted forward as the reaction of the other ejected backward as a fuel. The entire sequence of the processes causing *compression* and *explosion*, leading to the *acceleration* of bulk medium, are found to be highly stable and then robust without causing any serious instability even including the nonuniformity of laser intensity associated with a tight laser focal spot.

DOI: 10.1103/PhysRevResearch.7.013119

I. INTRODUCTION

Relativistic rocket is a fascinating challenge of boosting an object with finite mass and volume as an object (bulk medium) consisting of a large number of atomic nuclei to the level of the light speed c. The concept of the rocket is to release high-pressure heated fuel and corresponding momentum from the object at high speed, which creates a large reaction force to boost the remaining part forward by gaining nearly the same amount of momentum. A typical application is laser fusion [1,2], where a spherical target irradiated with a nanosecond high-power laser becomes a high-pressure plasma state, causing outward ablation. As a reaction for conserving momentum, shock waves are induced, propagating inward, while slowly compressing the target medium to higher density. A different approach that boosts an object (a bulk medium) [3] is proposed, where a high-power laser (microwave) is directed toward a rear-mounted parabola reflector. The laser is then reflected and focused back into free space, causing an explosive discharge and generating a shock, which strikes the object and creates thrust. In both cases, lasers are utilized to deliver a large amount of photon energy to the object, creating a high-energy density plasma state, whose dynamics, e.g., ablation, implosion, explosion, etc., produces a directed large momentum.

Recently, with the discovery of chirped pulse amplification (CPA) technologies [4–8], short pulse high-intensity lasers that confine light energy to the order of femtoseconds are being developed, reaching the intensity of 10^{21-22} W/cm^2 (so-called relativistic regime) at visible wavelengths. Such lasers are known to have the capability to provide a strong impact on a bulk medium, generating large amplitude nonlinear waves, e.g., shock waves, as mentioned above, but at a much higher level. In fact, such lasers have been used to accelerate ions (either protons or heavier ions) to high energies of tens to 100 MeV/u, e.g., aimed at compact accelerators for medical applications. Recently, a method has been proposed to realize wake-field acceleration of ions by moving the focal spot of light to generate collimated quasimonoenergetic ions of GeV/u [9]. Such significant progress and advantage of laser technology remind us to use them to realize a relativistic rocket. However, achieved maximum energies are still low compared to the light speed, and more importantly, the number of accelerated ions remains low as long as the methods that have been developed so far are used. Therefore, while taking advantage of such short-pulse lasers, it is necessary to explore a different scheme that can accelerate dense bulk medium to near the light speed. Based on this idea, here we utilize the above-mentioned CPA-based short pulse laser in a similar intensity regime but with a careful selection of parameters that regulate the interaction, e.g., laser pulse length and spatial

*Contact author: matsui.ryutaro.8r@kyoto-u.ac.jp
†Contact author: kishimoto.yasuaki.84r@st.kyoto-u.ac.jp

shaping, and most importantly, the target material and spatial configuration.

Meanwhile, such a laser has the unique capability to significantly modulate the produced relativistic plasma, which influences the plasma frequency $\omega_p \equiv (4\pi n_e e^2/m_e\gamma_e)^{1/2}$ (n_e: electron density; e: elementary charge; m_e: the electron mass; $\gamma_e \sim (1 + a_0^2/2)^{1/2}$: the electron relativistic factor; a_0: the normalized amplitude of laser) and the collisionless electron skin depth $\delta_e(= c/\omega_p)$ through the following two processes. One is that the laser is reflected by piling up electrons forward by the laser ponderomotive nonlinearity, causing a further denser plasma layer in front. The other is that the laser penetrates the plasma by expelling electrons aside or increasing the cutoff density n_c ($= \gamma_e n_{c0}$) by the relativistic nonlinearity [10,11], where n_{c0} represents the nonrelativistic cutoff density defined by $n_{c0} = m_e\omega^2/4\pi e^2$ with $\omega = 2\pi c/\lambda_L$. The former causes shock waves [12–16] in the medium, a kind of nonlinear wave, while the latter causes channeling [17,18].

To find such a scheme, we conduct a particle-in-cell (PIC) based simulation for the interaction between the high-intensity laser and solid hydrogen medium, taking the laser pulse shape and the target geometry as key factors. As a typical example, we use $\tau = 20\,\mathrm{fs}$ $(1/e)$ (Gaussian shape) with a rising time of 10 fs, which is nearly the shortest laser pulse width currently in development. As for the object irradiated by such lasers, we choose a solid hydrogen medium ($n_{e0} \sim 4.6 \times 10^{22}\,\mathrm{cm}^{-3}$) as the lightest object with a charge-to-mass ratio of unity among all substances, which is preferable for the present purpose causing a large acceleration. Such an object has been developed by a cryogenically cooled technology [19–22]. As the target geometry, we study two cases: one is the slab geometry and the other is a rod (string) geometry whose radius is in the same order as the laser wavelength λ_L.

In this paper, we propose a scheme to realize boosting a bulk medium, whose density reaches the level of the solid density, to the relativistic regime. In this scheme, due to the ultrashort ($\tau \sim 20\,\mathrm{fs}$) laser irradiation to the solid hydrogen medium, a peaked structure with a large amplitude ($\sim 18 n_{e0}$), whose width is narrower than the local Debye length, is induced. Then, an explosion of the structure is triggered by an induced electric field reaching 200 TV/m, which produces two shocks, i.e., one is a front shock boosted forward like a rocket, and the other is a latter shock ejected backward as a fuel. The front shock boosts the upstream bulk medium with the solid density to the sub-GeV regime. This scheme stably and robustly works for $0.5 \times 10^{22} \leqslant I \leqslant 2 \times 10^{22}\,\mathrm{W/cm^2}$, where the optimal intensity exists at $I \sim 1.0 \times 10^{22}\,\mathrm{W/cm^2}$.

In the series of simulations, we emphasize a parameter defined by ρ_e/γ_e ($\rho_e = en_e$), which directly affects $\omega_p \propto (\rho_e/\gamma_e)^{1/2}$, and then also $\delta_e \propto (\gamma_e/\rho_e)^{1/2}$, which regulates the propagation and attenuation of the laser field in dense plasmas. Here, ρ_e is normalized by en_{e0} in the following, so that $\rho_e/\gamma_e = 1$ in the absence of a laser field. We refer to ρ_e/γ_e as a *frozen-in parameter* [23] in the sense that ρ_e/γ_e tends to be less sensitive to the laser ponderomotive and relativistic nonlinearities in a high-intensity nonlinear regime. Namely, as the laser intensity increases, both ρ_e and γ_e increase simultaneously due to the above nonlinearities, so that the numerator and denominator in ρ_e/γ_e cancel each other. When ρ_e/γ_e becomes small ($\rho_e/\gamma_e < 1$), the intense laser field tends to penetrate the dense plasma by prolonging δ_e without sweeping off electrons and to propagate as a flowing plasma. This creates an extreme state in which highly compressed dense plasma and intense laser fields coexist and propagate stably, which is characterized as a function of a relativistic plasma. This is in contrast to the case where a high-intensity laser field is confined to a lower-density region surrounded by a higher-density plasma above the critical density, which results from a kind of structure resonance [24].

II. INTERACTION WITH HYDROGEN SLAB TARGET

Here, we study the case of two-dimensional (2D) slab geometry, which is rectangular in the (x, y) plane and uniform in the z-direction, for the solid hydrogen medium. Figure 1 illustrates three-dimensional (3D) images of ion (proton) charge density ρ_i, which also includes 1D distribution views (see figure caption). Owing to the ultrashort ($\tau \sim 20\,\mathrm{fs}$) and high-intensity laser irradiation and propagation in the $+y$ direction, a shocklike structure is generated, by which ρ_i increases rapidly, as seen in Figs. 1(a) and 1(b). In Fig. 1(c), a peaked structure of ions with $\rho_i \sim 18$ is formed at $y \sim 0$. The localized positive charge of the ions generates a bipolar electric field E_y with an intensity of up to 200 TV/m. The structure subsequently splits into two shocklike structures, where the front shock is largely boosted in the $+y$ direction as a *rocket* by ejecting the latter shock in the $-y$ direction as a *fuel*. This mechanism yields a high-energy bulk medium over 100 MeV within an extremely limited spatiotemporal scale of $\sim 1\,\mu\mathrm{m}$ and $\sim 10\,\mathrm{fs}$, as indicated by the arrow in Fig. 1(d). Finally, the front shock propagating in the $+y$ direction turns into a soliton with no reflection of the upstream ions and then small dissipation as shown in Fig. 1(e). In the following, we show the detailed dynamics by using the 1D cross-sectional view of (a) ρ_i for every 1.34 fs, (b) the longitudinal electric field E_y for times picked up from (a), and (c) temporal evolutions for ρ_{ip}, which indicates the peak value of ρ_i (black solid line) and position of y (blue dashed line) exhibiting ρ_{ip} in Fig. 2.

A. Bifurcation dynamics of nonlinear waves

When the laser hits the surface of the hydrogen medium at $t = 32.2\,\mathrm{fs}$, the laser ponderomotive force f_{PM} starts to push electrons forward, which induces the longitudinal electric field E_y exhibiting a positive monopole structure with even parity around the surface. Then, the ion medium is accelerated forward by E_y, which results in a quasi-1D shocklike structure (brown). As shown in the inset in Fig. 2(c), the peak value of ρ_i, which we define as ρ_{ip}, exhibits an approximately exponential growth $\rho_{ip} \sim \exp(\gamma t)$ in two phases, i.e., the growth rate $\gamma_{1\mathrm{st}} \sim 0.099/\mathrm{fs}$ in the first phase ($t = 36.2$–$41.5\,\mathrm{fs}$) and $\gamma_{2\mathrm{nd}} \sim 0.34/\mathrm{fs}$ in the second phase ($t = 45.5$–$50.9\,\mathrm{fs}$), which are connected through the stagnation phase. Due to the continuous compression of ρ_i, pushed electrons are pulled back as a reaction. As a result, E_y tends to stagnate or slightly decay (black), followed by the stagnation of ρ_{ip} at $t \sim 44.2\,\mathrm{fs}$. Since f_{PM} keeps working, E_y again increases (blue). These steps exhibit a *seesawlike relationship* where the ion dynamics and that of the longitudinal electric field are adiabatically coupled, constituting a *slow process*. After $t > 44.2$ fs, the similar seesaw dynamics are repeated, however, ρ_{ip} does not

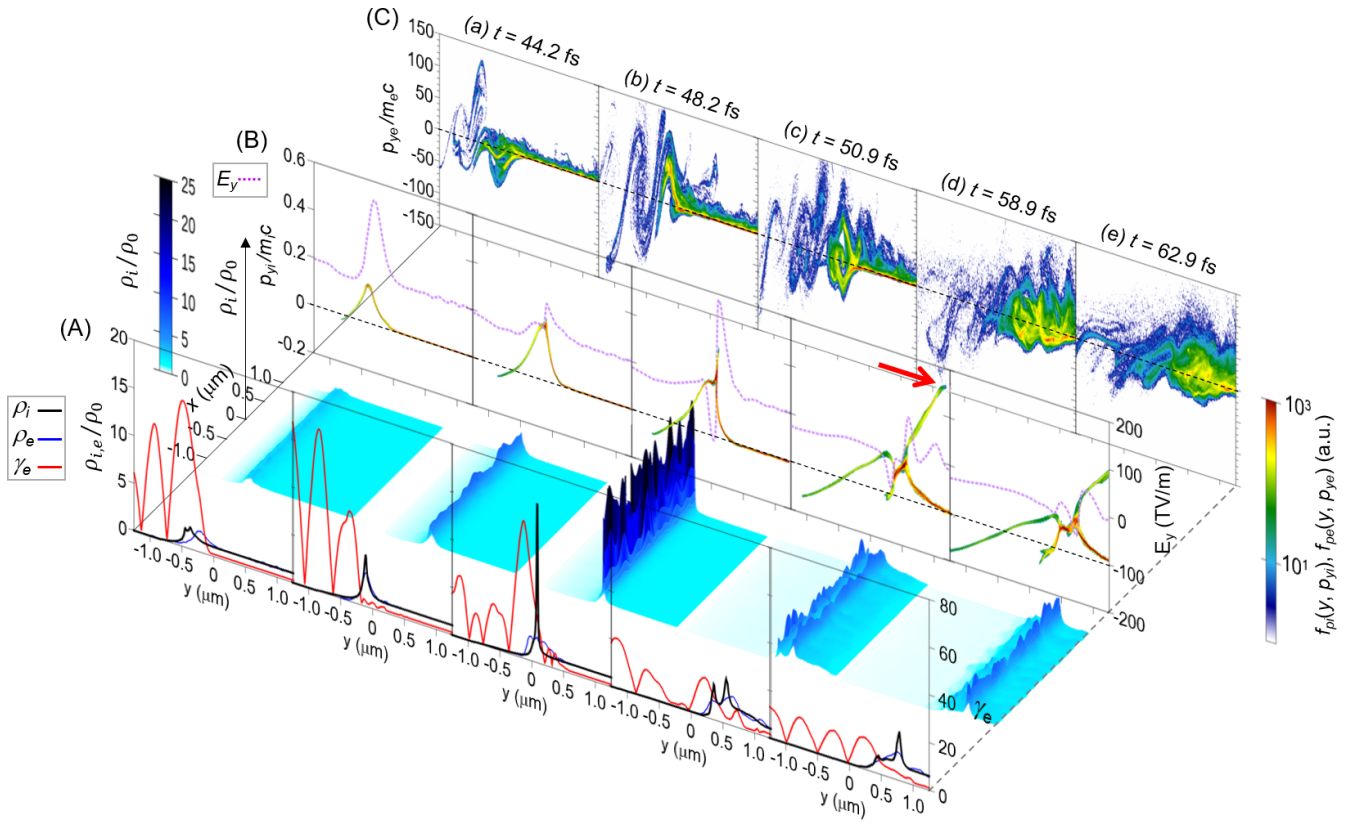

FIG. 1. Three-dimensional (3D) images of charge density distributions of ions ρ_i at five different times (a)–(e) after the laser irradiation. One-dimensional (1D) cross-sectional views averaged over x direction for (A) the ions ρ_i (black) and electrons ρ_e (blue) and the electron relativistic factor $\gamma_e = (1 + a_0^2/2)^{1/2}$ (red), (B) the longitudinal electric field E_y (purple) and corresponding phase space distributions of ions $f_{pi}(y,\ p_{yi})$, and (C) electrons $f_{pe}(y,\ p_{ye})$ in the y direction. ρ_i and ρ_e are normalized by the initial solid charge density $\rho_0 = en_{e0}$.

stagnate but keeps exponentially increasing up to $\rho_{ip} \sim 18$ at $t = 50.9$ fs (red). For $t > 44.2$ fs, the skin depth $\delta_e (= c/\omega_p) \propto (\gamma_e/\rho_e)^{1/2}$ is prolonged due to the rapid increase of the laser electric field $|E_x|$, which allows the laser to penetrate the compressed dense plasma. Consequently, the frozen-in condition discussed above is established and stably sustained, whose details are explained in the rod geometry (Fig. 5). From $t = 44.2$ to 50.9 fs, the width in the y direction around the peak of ρ_i is reduced one order of magnitude smaller from $\delta_y \sim 0.2$ μm (blue) to $\delta_y \sim 0.02$ μm (red), leading to a singular structure. Then, interestingly, from $t = 44.2$ to 50.9 fs, E_y changes the topology from even parity to odd parity, which causes an *explosion* explained in the following (b).

B. Explosion dynamics equivalent to rocket ignition and boosting

At $t \sim 50.9$ fs, the singular structure resulting from the bifurcation from shocklike to solitonlike structure *explodes* as a *fast process*, which is in contrast to the slow process mentioned above. This is because the width of the singular structure $\delta_y \sim 0.02$ μm becomes shorter than the local Debye length $\lambda_{de} \sim 0.08$ μm, so that a large field E_y with odd parity is induced due to a strong Coulomb force. Then, the solitonlike structure splits into two shocklike structures propagating in opposite directions at $t = 58.9$ fs [Figs. 1(d) and 2(a)]. The front shock is boosted forward as a *rocket* by the reaction of the latter shock ejected backward as a *fuel* [Figs. 1(d), 2(a), and 2(b)]. At the same time, the front shock boosts the upstream ions forward, which leads to the high-energy bulk medium in the relativistic regime. This boosting scheme is clearly shown in Fig. 3, which shows the 1D cross-sectional views of ρ_i and $f_{pi}(y,\ p_{yi})$ at $t = 50.9$ and 58.9 fs. The solitonlike structure (A), the front shock (B), the latter shock (C), and the high-energy bulk medium (D) are indicated, respectively. During the explosion process of the solitonlike structure with momentum $\boldsymbol{P}_{0,(A)}$, the latter shock is ejected backward with a momentum $\boldsymbol{P}_{ls,(C)}$ and the front shock gains a large forward momentum $\boldsymbol{P}_{fs,(B)}$, while it is quickly transferred to the high-energy bulk medium. Therefore, it is largely boosted forward with a momentum $\boldsymbol{P}_{r,(D)}$ to the entrance of the relativistic regime, where the conservation of relativistic momentum [25], i.e., $\boldsymbol{P}_{0,(A)} \sim \boldsymbol{P}_{fs,(B)} + \boldsymbol{P}_{ls,(C)} + \boldsymbol{P}_{r,(D)}$, are approximately satisfied. It is noted that the mass of the high-energy bulk medium (D) is equivalent to the initial solid hydrogen and reaches approximately 21% for the mass of the solitonlike structure (A) in Fig. 3. The efficiency leading to (D) from (A) is estimated as $\boldsymbol{P}_{r,(D)}/\boldsymbol{P}_{0,(A)} \sim 44\%$, which corresponds to almost half of the initial momentum $\boldsymbol{P}_{0,(A)}$. This indicates that an extremely large momentum transfer to the upstream bulk medium is realized, which is larger than those transferred to each front and latter shock. The detailed quantitative analysis is given in Appendix B. Here, the front shock only plays a role as a momentum transmitter to the high-energy bulk medium.

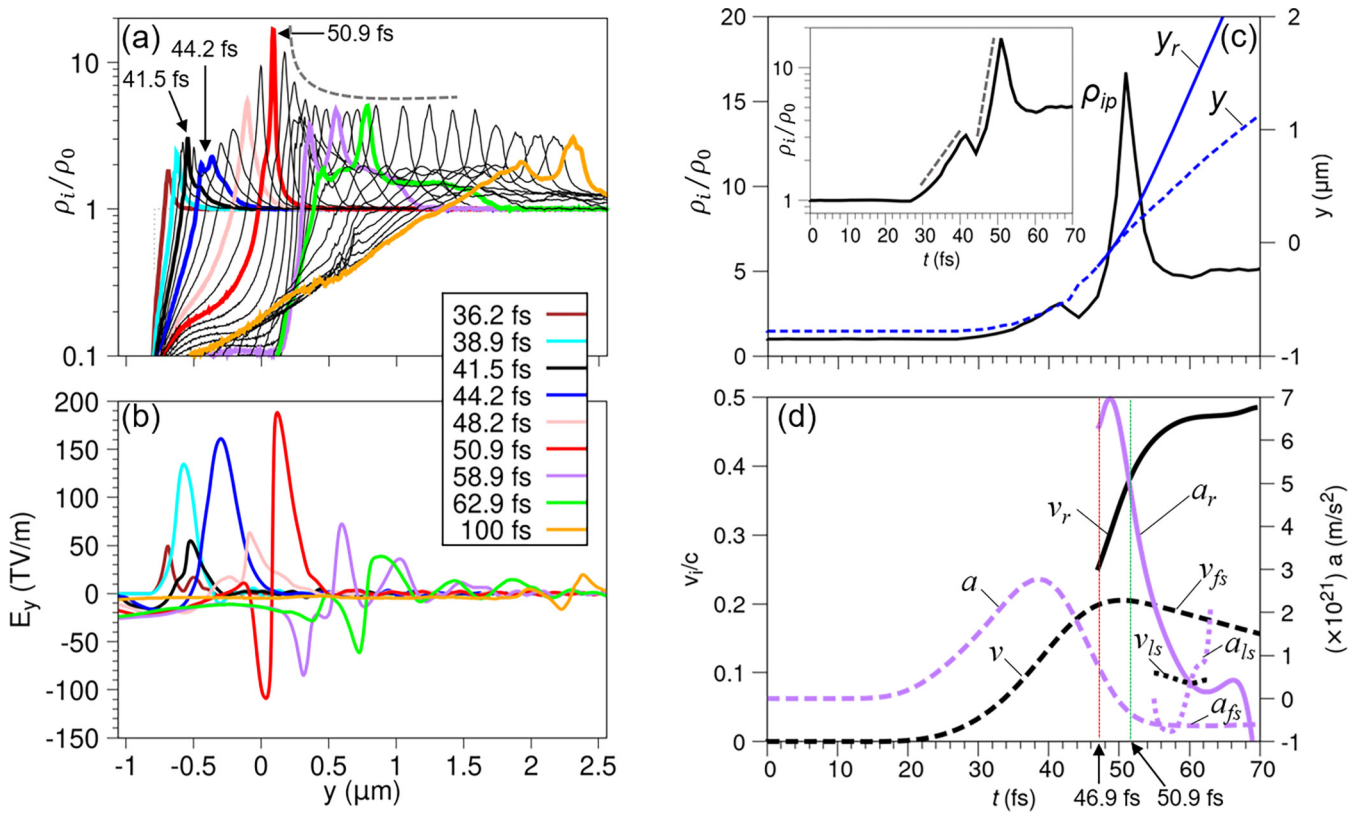

FIG. 2. 1D cross-sectional view of (a) successive charge density of ions ρ_i for $t = 36.2 - 100$ fs and (b) corresponding electric field E_y. (c) Temporal evolutions for the locations y (the peaked structure), y_r (the boosted ion medium front), and ρ_{ip}. ρ_i and E_y are averaged along the x direction. (d) Temporal evolutions for accelerations a and velocities v of the shocklike peaked structure, and also those of bifurcated front and latter shocks, $(a_{fs},\ v_{fs})$ and $(a_{ls},\ v_{ls})$, respectively after $t = 50.9$ fs, and also those of pushed upstream bulk medium, $(a_r,\ v_r)$ after $t = 46.9$ fs, shortly before the explosion. The velocities are normalized by c. The velocities and accelerations are smoothed by using the Bezier curve.

Here, it is worth noting the maximum momentum of protons obtained by the present boosting mechanism. Under the condition that the Hamiltonian is conserved for a given electrostatic potential structure moving with a constant drift velocity, the obtained maximum momentum of ions $p_{y.\max}$ can be estimated. When we apply the model presented in Ref. [26] to the present case, i.e., the drift velocity is $v_d = 0.21c$ and the potential energy is $e\phi \sim 61.4$ MeV at $t = 50.9$ fs [Fig. 3(a)], we get the momentum $p_{y.\max} \sim 0.61\, m_i c$, which is close to the value of $0.54 m_i c$ [see p_{yi} at $y \sim 1.3$ μm in Fig. 3(b)]. The detailed analysis is given in Appendix B.

C. Remnant dynamics by soliton and rarefaction waves after explosion

However, a short time later (~ 4.0 fs), at $t = 62.9$ fs, the front shock propagating forward changes the topology again to a soliton structure with E_y exhibiting a bipolar

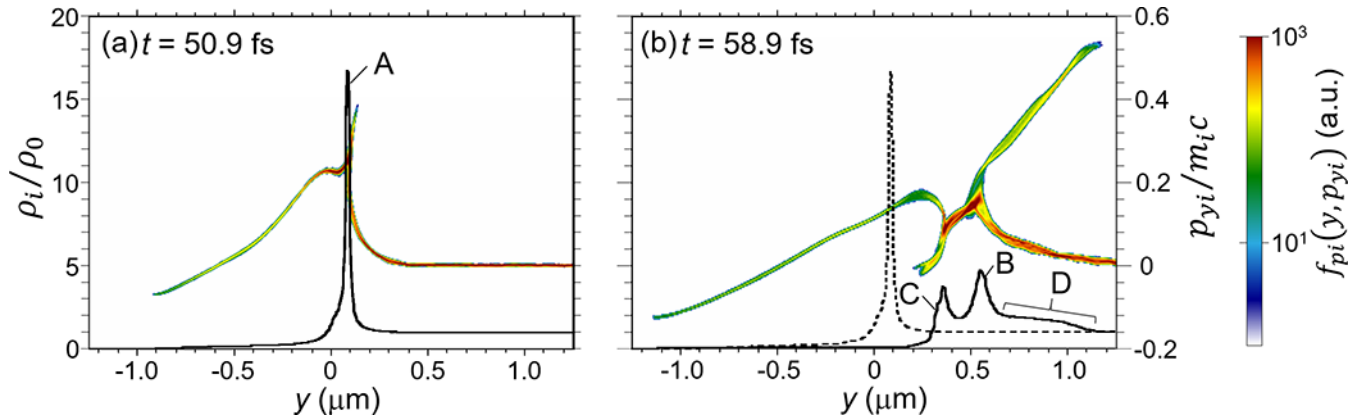

FIG. 3. Two-dimensional (2D) images of ρ_i and corresponding phase space distributions of ions $f_{pi}(y, p_{yi})$ at (a) $t = 50.9$ fs and (b) $t = 58.9$ fs. The solitonlike structure (A), which initially moves in the $+y$ direction, turns into the front shock (C) by ejecting the latter shock (B) backward and the high-energy bulk medium (D) forward.

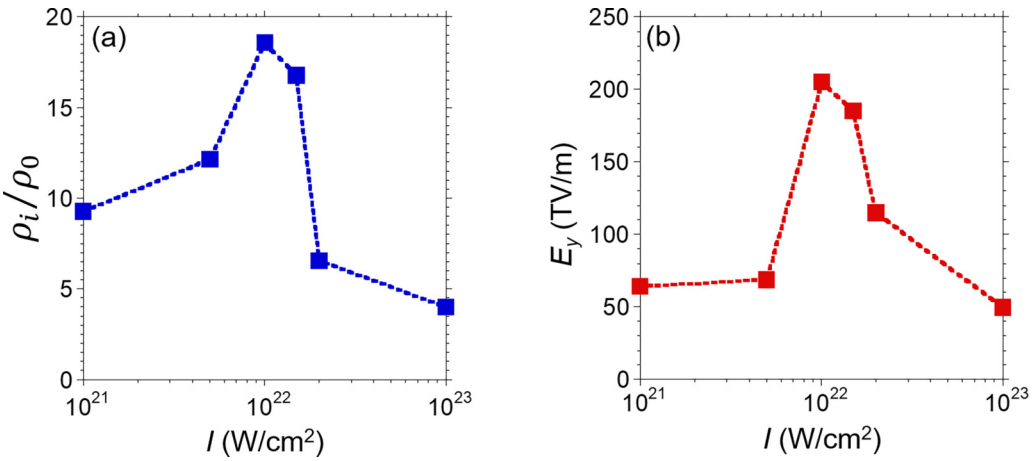

FIG. 4. (a) The maximum density of ions ρ_i for different laser peak intensity I. (b) The value of the longitudinal electric field E_y associated with the shocklike/solitonlike structure for different laser peak intensity I.

structure with even parity, which means the end of the boosting. The soliton structure propagates stably with $v_{\rm fs} \sim 0.13c$ [Figs. 2(a), 2(b), and 2(d)]. On the other hand, the latter shock is absorbed into the rarefaction wave triggered at $t \sim 62.9$ fs from the sharp edge. The edge of the rarefaction wave propagates in the $+y$ direction paired with the soliton, which are both remnants propagating with the local sound speed and survive for a longer time in the medium after the explosive event.

D. Effect of laser intensity I on the boosting scheme

In order to confirm the stability of the present boosting scheme, we investigate the dependence of the laser intensity I on the compression of ρ_i and the intensity of E_y across two orders of magnitude from 1.0×10^{21} to 1.0×10^{23} W/cm^2 for the same pulse width and shape. From the fact that the entire sequence of present acceleration dynamics (compression, and subsequent explosion and acceleration) occurs within 1 μm from the solid surface as seen in Fig. 2, here, for simplicity, we shorten the slab width in the y direction from 5 to 1.6 μm ($-0.8 \leqslant y \leqslant 0.8$ μm), for simplicity Here, Fig. 4(a) shows the peak charge density ρ_i, corresponding to ρ_{ip} in Fig. 2(c), which provides the maximum compression rate, and Fig. 4(b) shows the peak value of E_y associated with the shocklike/solitonlike structure for the different laser intensity I.

For the former lower intensity case, the shocklike structure with monopole field E_y is induced. However, the laser field hardly penetrates the dense plasma due to the relatively lower laser intensity I, so that the frozen-in condition is not established. Instead, the upstream ions are simply accelerated by the shock structure. This is considered to be the acceleration dynamics referred to as collisionless shock acceleration (CSA). For the latter higher intensity case, the shocklike structure is also induced, however, the laser fields penetrate the dense plasma before ρ_i grows exponentially [up to 4 in Fig. 4(a)], which leads to the establishment of the pressure balance in the moving frame, i.e., the high-pressure bulk electrons are sandwiched by the intense laser antinodes and laser pushes them in the $+y$ direction like a *piston*. This state shows a resemblance with a kind of structure resonance [24], which is in contrast to the frozen-in state. However, the intensity of E_y is 50 TV/m [Fig. 4(b)] and the obtained maximum energy of ions is at most several tens MeV even though the laser is an order of magnitude higher. From these results, there is a region of intensity I that the present boosting scheme works for given pulse length and shape.

III. INTERACTION WITH HYDROGEN ROD TARGET

Here, we extend the study using the slab geometry to that of a 2D rod, which is circular in the (x, y) plane and uniform in the z-direction, with the radius $R = 0.8$ μm, which is roughly the same as λ_L. Figure 5 illustrates 2D images for ρ_e [Figs. 5(a)–5(e)] and ρ_i [Figs. 5(f)–5(j)], respectively, with γ_e (white) and ρ_e/γ_e (orange). After the laser hits the target, ρ_e exhibits a global distortion on the scale of R with broadband turbulencelike fluctuation that contains multiple spiky structures in front of the laser field. Figure 5(k) illustrates the 1D profiles ρ_i at successive different times. Namely, the peak value ρ_{ip} also increases exponentially in two phases with a period of stagnation at $t \sim 44.2$ fs. The growth rates of the first phase ($t = 36.2$–41.5 fs) and the second phase ($t = 45.5$–49.6 fs) are estimated as $\gamma_{\rm 1st} \sim 0.11$/fs and $\gamma_{\rm 2nd} \sim 0.37$/fs, respectively, which are similar levels as in the slab case.

After the stagnation period, multiple spiky structures of ρ_e [Fig. 5(b)] tend to coalesce near the center region of the rod [Fig. 5(c)] along the concave structure of ρ_i [Fig. 5(g)]. Accordingly, ρ_i is evolved exhibiting a sheet structure in the x direction whose length is $\ell_s \sim 0.4$ μm ($\sim 0.5\,\lambda_L$), while compressed to $\rho_{ip} \sim 18$ with narrowing the width in the y direction at $y \sim 0$ in Fig. 5(h). Note that the *seesaw* dynamics between ρ_{ip} and E_y discussed in the slab case are also responsible for causing a peaked sheet structure. Around the time that ρ_{ip} reaches the maximum value, E_y changes the topology transiently from shocklike to solitonlike, followed by an *explosion* causing two shocks. The former one is further boosted as the front shock.

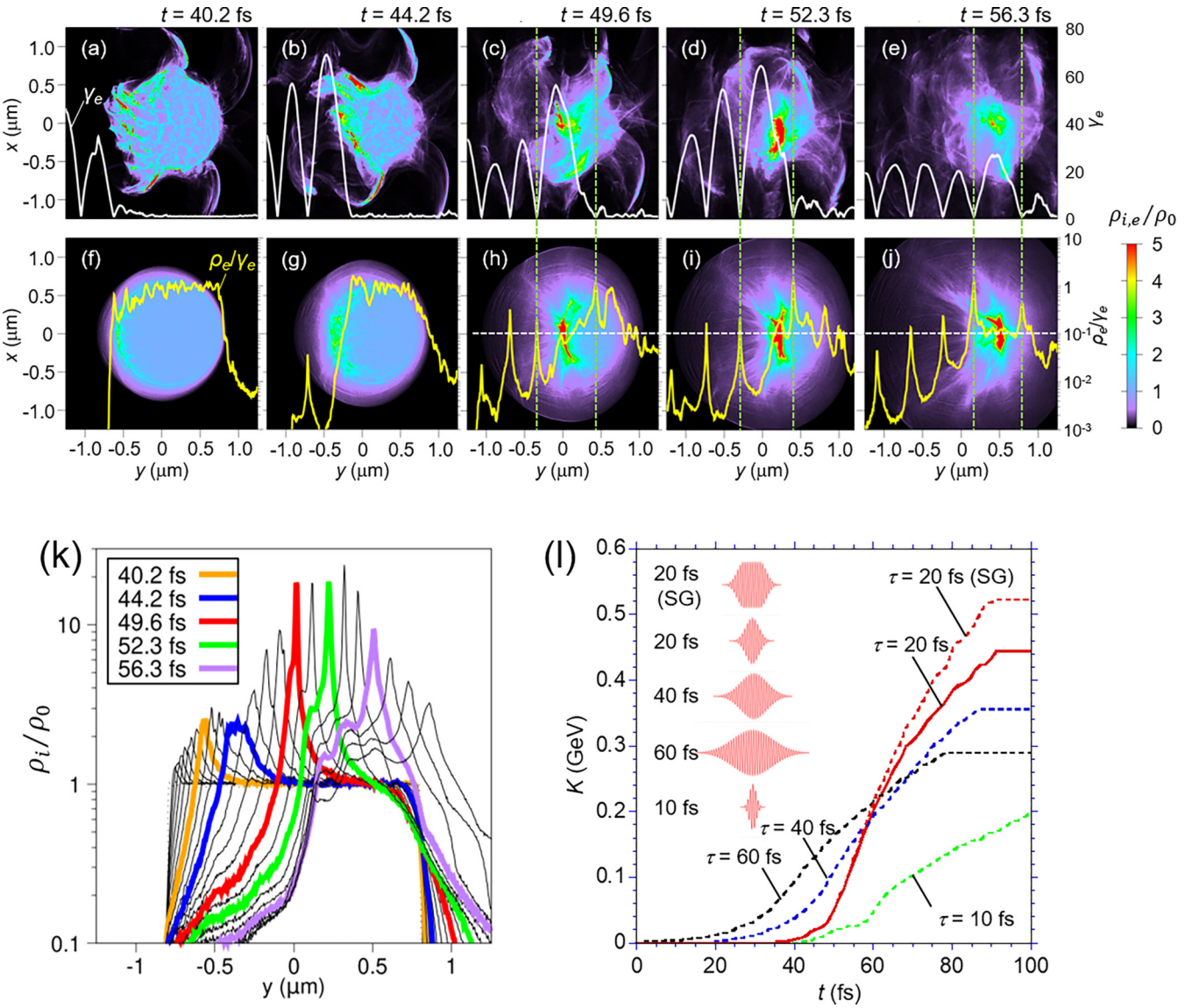

FIG. 5. 2D images of charge density distributions of (a)–(e) electrons ρ_e and (f)–(j) ions ρ_i. The electron relativistic factor $\gamma_e = (1 + a_0^2/2)^{1/2}$ (white) and the frozen-in parameter $\rho_e/\gamma_e \sim \omega_p^2$ (yellow) are also shown. γ_e and ρ_e/γ_e are averaged over $-0.08 < x < 0.08\,\mu$m in the x direction. (k) 1D cross-sectional view of successive charge density of ions ρ_i. (l) Temporal evolutions for the maximum proton energy K at $\tau = 10$, 20, 20 (supper-Gaussian), 40, and 60 fs with the same I. The pulse shapes for each case are also shown.

A. Stability of the frozen-in parameter ρ_e/γ_e

Here, we found the change of frozen-in parameter ρ_e/γ_e across the stagnation time ($t \sim 44.2$ fs), after which the exponential growth of ρ_{ip} is rebuilt as seen in Figs. 5(f)–5(h). Here, ρ_e is normalized by en_{e0} in the following, so that $\rho_e/\gamma_e = 1$ in the absence of a laser field. Namely, as the laser intensity increases, both ρ_e and γ_e increase simultaneously, so that the numerator and denominator in ρ_e/γ_e cancel each other. In the first phase, e.g., at $t = 40.2$ fs [Fig. 5(f)], the condition $\rho_e/\gamma_e \sim 1$ is established since the laser field does not penetrate the semicircle including the concave region. However, at $t = 44.2$ fs [Fig. 5(g)], which is the time that the second phase starts, the condition $\rho_e/\gamma_e \ll 1$ is established, where the laser field with $\gamma_{e,\max} \sim 60$ ($\sim a_0$) starts to penetrate the denser region of ρ_e ($\sim \rho_{ep} \sim 20$). After $t > 44.2$ fs [Figs. 5(h)–5(j)], the location of the peaked sheet structures of ρ_e and ρ_i coincides with that exhibiting the maximum value of the laser field $|E_x|$, and then copropagates with each other quasicoherently without causing scattering/thermalization [Figs. 1(c)–1(e) in (C)], where ρ_e/γ_e is frozen to almost the constant value around $\rho_e/\gamma_e \sim 0.1$. This state is maintained with robustness, which may result from the nearly constant nature of $\rho_e/\gamma_e \propto \omega_p^2 \propto 1/\delta_e^2$ in regulating the electromagnetic dispersion even in the presence of strong laser fields. Supported by the stability of ρ_e/γ_e, the front shock pushes the upstream bulk medium forward, generating a high-energy component with the velocity $v_r \sim 0.57c$ (200 MeV) at $t \sim 60$ fs, which is similar dynamics to the slab case. Here, the velocity of the front shock is boosted from $v \sim 0.23c$ to $v_{\rm fs} \sim 0.25c$. This is because the mass of the high-energy component is much smaller than that of the front shock due to the limited mass of the rod structure, so only a part of the front shock's momentum is transferred to the high-energy component.

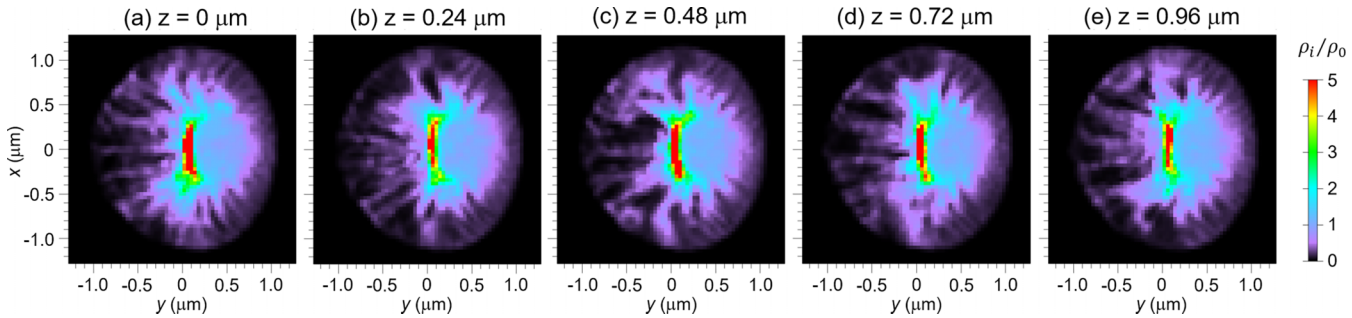

FIG. 6. The 2D cross-sectional views of ρ_i at intervals of 0.24 μm from $z = 0$ to $z = 0.96$ μm at $t \sim 49.6$ fs, which is the time that the explosion takes place.

B. Effect of pulse width τ on the boosting scheme

Figure 5(l) shows the temporal evolutions for the front energy corresponding to the high-energy component estimated by that of a representative proton K as a measure of the performance of the presented boosting scheme for different shapes of the incident laser. The energy K for the present laser of $\tau = 20$ fs suddenly increases due to the boost of the front shock by the explosion at $t \sim 50$ fs and reaches 0.3 GeV at $t \sim 70$ fs, followed by the boost of the high-energy component. After $t > 70$ fs, the high-energy component is further boosted by the sheath field E_y induced at the rod surface, leading to 0.44 GeV. For the super-Gaussian (SG) shape with the same rising time of 10 fs, the growth rate of K is almost the same as that of $\tau = 20$ fs in $t < 60$ fs, indicating that the rising time is a key to the present boosting scheme. For the longer laser pulse of $\tau = 40$ and 60 fs, no ignition takes place, and it is less boosted [15]. The growth rate of K for $\tau = 20$ fs is approximately twice compared with those for $\tau = 40$ and 60 fs, even though the pulse energy is less than half. The initial formation of a shocklike structure fails for the shorter laser pulse of $\tau = 10$ fs.

C. Stability for 3D rod geometry

So far, we have studied 2D geometries assuming uniformity in the z direction, while a case can be considered that the medium irradiated by such high-intensity lasers loses stability in the z direction even if the laser is uniform, such as kink and/or sausagelike distortions, which prevents higher density compression before the explosion takes place. For this purpose, here, we perform full 3D simulations, including the freedom of distortion in the z-direction, by setting the solid hydrogen medium of the same radius $R = 0.8$ μm with the height of $h = 2.0$ μm using the periodic boundary condition. In Figs. 6(a)–6(e), we show the 2D cross-sectional views of ρ_i at intervals of 0.24 μm from $z = 0$ to $z = 0.96$ μm at $t \sim 49.6$ fs, which is the time that the explosion takes place. It is found that the similar sheet structure with the length of $\ell_s \sim 0.7$ μm is formed in the x direction, followed by the subsequent explosion and acceleration at the same timing as those observed in the 2D case [Figs. 5(h)–5(j)] without causing any significant distortion with the order of 1 μm in the z direction. These results indicate that the series of dynamics leading to the explosion and acceleration are stable and robust.

IV. CONCLUDING REMARKS

In this work, we discovered a function of a relativistic plasma dominated by the frozen-in condition that the parameter ρ_e/γ_e regulating the dispersion through the plasma frequency ω_p and electron collisionless skin depth δ_e weakly depends on laser ponderomotive and relativistic nonlinearities due to their cancellation in the highly nonlinear regime. This makes it possible to create a different extreme state in which highly compressed dense plasma and intense laser fields coexist stably. By utilizing this state, we realized an explosion in the solid hydrogen medium and boosting the bulk medium to near the light speed aiming at a relativistic bulk medium. The mechanism is found to work only in the hydrogen medium with a charge-to-mass ratio of unity among all substances in nature. When we use the solid deuterium slab/rod with the same electron density as solid hydrogen, the shocklike structure is not induced and the present boosting scheme does not work. This is because the deuterium ions hardly follow the electrons pushed forward by the strong ponderomotive force due to their large mass. To explore the target with materials heavier than solid hydrogen is key to expanding the range of applications.

ACKNOWLEDGMENTS

This work was supported by Grant-in-Aid for Scientific Research (A) Grant No. 17H01180, (A) Grant No. 21H04452, Grant-in-Aid for Research Activity Start-up Grant No. 20K22329, Grant-in-Aid for Early-Career Scientists Grant No. 22K14019 by JSPS KAKENHI, the Collaborative Research Program of Institute for Chemical Research, Kyoto University (Grants No. 2023-128 and No. 2024-121), the ZE Research Program, IAE (Grants No. ZE2024B-14, No. ZE2024B-31, and No. ZE2024D-1), and SPIRITS 2021 of Kyoto University.

APPENDIX A: NUMERICAL MODELING

Simulations are performed using the two-dimensional (2D) version of the particle-based integrated code EPIC3D [15,16,27]. The system has a dimension of $L_x \times L_y = 5.12 \times 10.24$ μm containing 1024×2048 cells, and the coordinates are set to $-2.56 \leqslant x \leqslant 2.56$ μm and $-2.56 \leqslant y \leqslant 7.68$ μm. A cell size of 5 nm is used to resolve the nonlinear structures in detail. To explain the fundamentals of a boosting scheme,

a solid hydrogen slab is set, which consists of solid-density hydrogen molecules with an electron density of $n_e(\rho_{e0}) = 4.6 \times 10^{22}\,\mathrm{cm}^{-3} \sim 26.8\,n_c$. The hydrogen slab occupies an area of $-2.56 \leqslant x \leqslant 2.56\,\mu\mathrm{m}$ and $-0.80 \leqslant y \leqslant 4.20\,\mu\mathrm{m}$, with a slab length of 5.0 μm. Furthermore, a solid hydrogen rod with a radius $R = 0.8\,\mu\mathrm{m}$ is set, with the rod center placed at $(x,\ y) = (0,\ 0)$. The number of PIC particles used for the ions is 60 and 280 per cell for the hydrogen slab and rod, respectively. Fully ionized and collisionless plasma is used as the initial condition. A linearly polarized laser pulse in the x direction (plane wave), with a pulse width of $\tau = 20$ fs ($1/e$), is generated from an antenna located at $y = -2.55\,\mu\mathrm{m}$ ($x = 0$). The pulse propagates in the $+y$ direction from $t = 0$, with a pulse energy $E \sim 5$ J. In this study, pulse width plays an essential role in the collisionless shocklike structure and resultant boosting, whereas pulse energy depends weakly on these dynamics. The peak intensity of the laser pulse is set to $I = 1.0 \times 10^{22}\,\mathrm{W/cm}^2$, which corresponds to $a_0 = 69.3$. The laser parameters are based on the currently available laser system with a contrast ratio of $\sim 10^{-9}$ [6,7]. For fields and particles, a periodic boundary condition is employed in the x direction and a transparent boundary condition is employed in the y direction. As shown in Fig. 1, the 3D images for different ρ_i are smoothened using fast Fourier transform processing. The densities ρ_i and ρ_e, the electron relativistic factor γ_e, and the field E_y are averaged in the x direction over $-2.56 \leqslant x \leqslant 2.56\,\mu\mathrm{m}$ and phase space distributions of ions $f_{pi}(y,\ p_{yi})$ and electrons $f_{pe}(y,\ p_{ye})$ in the y direction are averaged over $-0.08 \leqslant x \leqslant 0.08\,\mu\mathrm{m}$. The momenta of ions p_{yi} and electrons p_{ye} are normalized by $m_i c$ and $m_e c$, respectively.

For the 3D3V simulation in the case of the rod target, the system size is set to $L_x \times L_y \times L_z = 5.12 \times 5.12 \times 2\,\mu\mathrm{m}$ containing $128 \times 128 \times 50$ cells and the coordinates are set to $-2.56 \leqslant (x,\ y) \leqslant 2.56\,\mu\mathrm{m}$ and $-1.0 \leqslant z \leqslant 1.0\,\mu\mathrm{m}$. A hydrogen rod with a radius of $R = 0.8\,\mu\mathrm{m}$ and a height of $h = 2\,\mu\mathrm{m}$ is located at the center of the simulation box, i.e., the center of the rod is $(x,\ y) = (0,\ 0)$ and the rod axis is parallel to the z direction, with a periodic boundary condition in the x and z directions, while a transparency boundary condition is in the y direction.

APPENDIX B: DETAILED EVALUATION OF MOMENTUM CONSERVATION IN THE SLAB GEOMETRY

In the following, we evaluate the momentum conservation in the relativistic regime by using Figs. 2(d) and 3. At the moment of the *explosion* or shortly before ($t \sim 46.9$ fs), the upstream bulk medium is pushed forward with a larger acceleration. Through this process, a new high-energy component originating from the pushed upstream bulk medium is established, which corresponds to the initiation of a *second boosting* as shown in Fig. 2(d), which illustrates the temporal evolution of accelerations a and velocities v for various structures (details are in the figure caption). The velocity v increases in the slow process due to the large acceleration ($t \sim 36.2$ fs), while it saturates to the maximum value toward the time of the explosion ($t \sim 50.9$ fs). Then, v_{fs} turns to decrease, while v_r further increases, reaching $v_r \sim 0.47c$ (128 MeV).

The momentum $\boldsymbol{P}_{0,(\mathrm{A})}$ (corresponding mean velocity $\overline{\boldsymbol{v}_0} \sim 0.16c$) at $t = 50.9$ fs is transferred to $\boldsymbol{P}_{fs,(\mathrm{B})} \sim 0.32\boldsymbol{P}_{0,(\mathrm{A})}$ ($\overline{\boldsymbol{v}_{fs}} \sim 0.11c$), $\boldsymbol{P}_{ls,(\mathrm{C})} \sim 0.22\boldsymbol{P}_{0,(\mathrm{A})}$ ($\overline{\boldsymbol{v}_{ls}} \sim 0.096c$), and $\boldsymbol{P}_{r,(\mathrm{D})} \sim 0.44\boldsymbol{P}_{0,(\mathrm{A})}$ ($\overline{\boldsymbol{v}_r} \sim 0.35c$) at $t = 58.9$ fs, which roughly satisfies the conservation of relativistic momentum [25], i.e., $\boldsymbol{P}_{0,(\mathrm{A})} \sim \boldsymbol{P}_{1\mathrm{st-rocket},(\mathrm{B})} + \boldsymbol{P}_{\mathrm{fuel},(\mathrm{C})} + \boldsymbol{P}_{2\mathrm{nd-rocket},(\mathrm{D})}$. The velocities $\overline{\boldsymbol{v}_0}$ and $\overline{\boldsymbol{v}_{ls}}$ satisfy the Einstein velocity addition law given by $\overline{\boldsymbol{v}_{ls}} = (\boldsymbol{w}_a + \overline{\boldsymbol{v}_0})/(1 + \boldsymbol{w}_a\overline{\boldsymbol{v}_0}/c^2)$ at $t = 50.9$ fs, where $\boldsymbol{w}_a$ is the relative velocity of (C) to (A). Similarly, the velocities $\overline{\boldsymbol{v}_{fs}}$ and $\overline{\boldsymbol{v}_r}$ satisfy the relation given by $\overline{\boldsymbol{v}_r} = (\boldsymbol{w}_b + \overline{\boldsymbol{v}_{fs}})/(1 + \boldsymbol{w}_b\overline{\boldsymbol{v}_{fs}}/c^2)$ at $t = 58.9$ fs, where $\boldsymbol{w}_b$ is the relative velocity of (D) to (B). From these relations, $\boldsymbol{w}_a = -0.065c$ and $\boldsymbol{w}_b = +0.25c$ are estimated, indicating that the latter shock is ejected to the $-y$ direction, while the high-energy component is boosted to the $+y$ direction.

Here, it is worth noting the maximum momentum of protons $p_{y.\max}$ obtained by the present boosting mechanism. When the explosion takes place (at $t = 50.9$ fs), the electrostatic potential associated with the solitonlike structure (A) moves in the $+y$ direction with a drift velocity $v = 0.21c$. The maximum momentum of protons $p_{y.\max}$ by the reflection of such a *moving* electrostatic potential $e\phi$ is estimated by the following relations based on the Hamiltonian dynamics [26]:

$$\frac{p_{y,\max}}{m_i c} = \frac{\beta_d B + \sqrt{B^2 + \beta_d^2 - 1}}{1 - \beta_d^2}, \qquad B = \frac{e\phi_{\max}}{m_i c^2} + \sqrt{1 - \beta_d^2}, \tag{1}$$

where m_i is the proton mass and $e\phi_{\max}$ is the maximum value of the electrostatic potential obtained by integrating E_y from $y = 0.99\,\mu\mathrm{m}$ to $y = 0$ in the $-y$ direction [see the red line in Fig. 2(b)]. Here, $e\phi(y = 0.99\,\mu\mathrm{m}) = 0$ and $E_y(y = 0.99\,\mu\mathrm{m}) = 0$ are satisfied. The value β_d is the drift velocity of the potential normalized by the light speed c. In the present case, $e\phi_{\max}$ and β_d at $t = 50.9$ fs are estimated as 61 MeV and 0.21, respectively. By substituting these values into Eq. (1), $p_{y.\max}$ is estimated to be $0.61 m_i c$, which is close to the maximum momentum of $0.54 m_i c$ at $t = 58.9$ fs [see p_{yi} at $y \sim 1.3\,\mu\mathrm{m}$ in Fig. 3(b)]. Furthermore, for the condition that the reflection of upstream ions takes place, the values $e\phi_{\max}$ and β_d must satisfy the following relation [26]:

$$\beta_d < \beta^* \equiv \sqrt{2\frac{e\phi_{\max}}{m_i c^2} - \left[\frac{e\phi_{\max}}{m_i c^2}\right]^2}. \tag{2}$$

In the present case, β^* is estimated to be $0.36c$, which satisfies $\beta_d < \beta*$, indicating that the reflection of upstream ions should take place.

[1] R. Betti and O. Hurricane, Inertial-confinement fusion with lasers, Nat. Phys. **12**, 435 (2016).

[2] C. A. Williams *et al.*, Demonstration of hot-spot fuel gain exceeding unity in direct-drive inertial confinement fusion implosions, Nat. Phys. **20**, 758 (2024).

[3] Y. Oda, K. Komurasaki, K. Takahashi, A. Kasugai, and K. Sakamoto, Plasma generation using high-power millimeter-

wave beam and its application for thrust generation, J. Appl. Phys. **100**, 113307 (2006).

[4] D. Strickland and G. Mourou, Compression of amplified chirped optical pulses, Opt. Commun. **56**, 219 (1985).

[5] S. Tokita, M. Hashida, S. Masuno, S. Namba, and S. Sakabe, 0.3% energy stability, 100-millijoule-class, Ti:Sapphire chirped-pulse eight-pass amplification system, Opt. Express **16**, 14875 (2008).

[6] A. S. Pirozhkov *et al.*, Approaching the diffraction-limited, bandwidth-limited Petawatt, Opt. Express **25**, 20486 (2017).

[7] H. Kiriyama, Y. Miyasaka, A. Sagisaka, K. Ogura, M. Nishiuchi, A. S. Pirozhkov, Y. Fukuda, M. Kando, and K. Kondo, Experimental investigation on the temporal contrast of pre-pulses by post-pulses in a petawatt laser facility, Opt. Lett. **45**, 1100 (2020).

[8] C. Radier *et al.*, 10 PW peak power femtosecond laser pulses at ELI-NP, High Power Laser Sci. Eng. **10**, e21 (2022).

[9] Z. Gong, S. Cao, J. P. Palastro, and M. R. Edwards, Laser wakefield acceleration of ions with a transverse flying focus, Phys. Rev. Lett. **133**, 265002 (2024).

[10] S. Palaniyappan *et al.*, Dynamics of relativistic transparency and optical shuttering in expanding overdense plasmas, Nat. Phys. **8**, 763 (2012).

[11] S. Palaniyappan, C. Huang, D. C. Gautier, C. E. Hamilton, M. A. Santiago, C. Kreuzer, A. B. Sefkow, R. C. Shah, and J. C. Fernández, Efficient quasi-monoenergetic ion beams from laser-driven relativistic plasmas, Nat. Commun. **6**, 10170 (2015).

[12] L. O. Silva, M. Marti, J. R. Davies, R. A. Fonseca, C. Ren, F. Tsung, and W. B. Mori, Proton shock acceleration in laser-plasma interactions, Phys. Rev. Lett. **92**, 015002 (2004).

[13] A. Macchi, F. Cattani, T. V. Liseykina, and F. Cornolti, Laser acceleration of ion bunches at the front surface of overdense plasmas, Phys. Rev. Lett. **94**, 165003 (2005).

[14] D. Haberberger, S. Tochitsky, F. Fiuza, C. Gong, R. A. Fonseca, L. O. Silva, W. B. Mori, and C. Joshi, Collisionless shocks in laser-produced plasma generate monoenergetic high-energy proton beams, Nat. Phys. **8**, 95 (2012).

[15] R. Matsui, Y. Fukuda, and Y. Kishimoto, Quasimonoenergetic proton bunch acceleration driven by hemispherically converging collisionless shock in a hydrogen cluster coupled with relativistically induced transparency, Phys. Rev. Lett. **122**, 014804 (2019).

[16] R. Matsui, Y. Fukuda, and Y. Kishimoto, Dynamics of the boundary layer created by the explosion of a dense object in an ambient dilute gas triggered by a high power laser, Phys. Rev. E **100**, 013203 (2019).

[17] S. V. Bulanov, M. Lontano, T. Z. Esirkepov, F. Pegoraro, and A. M. Pukhov, Electron vortices produced by ultraintense laser pulses, Phys. Rev. Lett. **76**, 3562 (1996).

[18] N. M. Naumova, S. V. Bulanov, K. Nishihara, T. Z. Esirkepov, and F. Pegoraro, Polarization effects and anisotropy in three-dimensional relativistic self-focusing, Phys. Rev. E **65**, 045402(R) (2002).

[19] S. Garcia, D. Chatain, and J. P. Perin, Continuous production of a thin ribbon of solid hydrogen, Laser Part. Beams **32**, 569 (2014).

[20] D. Margarone *et al.*, Proton acceleration driven by a nanosecond laser from a cryogenic thin solid-hydrogen ribbon, Phys. Rev. X **6**, 041030 (2016).

[21] J. Polz *et al.*, Efficient laser-driven proton acceleration from a cryogenic solid hydrogen target, Sci. Rep. **9**, 16534 (2019).

[22] S. Jinno *et al.*, Laser-driven multi-MeV high-purity proton acceleration via anisotropic ambipolar expansion of micron-scale hydrogen clusters, Sci. Rep. **12**, 16753 (2022).

[23] L. N. Tsintsadze, T. Tajima, K. Nishikawa, J. K. Koga, K. Nakagawa, and Y. Kishimoto, Generation of low-frequency electromagnetic waves by spectrally broad intense laser pulses in a plasma, Phys. Scr. **T84**, 94 (2000).

[24] Y. Kishimoto, T. Watanabe, H. Hojo, and K. Nishikawa, Numerical method for nonlinear wave propagation and application to laser-plasma interaction, J. Phys. Soc. Jpn. **51**, 2304 (1982).

[25] F. Robert, A transparent derivation of the relativistic rocket equation, in *Proceedings of the 31st Joint Propulsion Conference and Exhibit, 10-12 July 1995, San Diego, CA* (AIAA, Reston, VA, 1995).

[26] Z. Gong, Y. Shou, Y. Tang, R. Hu, J. Yu, W. Ma, C. Lin, and X. Yan, Proton sheet crossing in thin relativistic plasma irradiated by a femtosecond petawatt laser pulse, Phys. Rev. E **102**, 013207 (2020).

[27] Y. Kishimoto, T. Masaki, and T. Tajima, High energy ions and nuclear fusion in laser–cluster interaction, Phys. Plasmas **9**, 589 (2002).